Proceedings of 2004 IEEE/RSJ International Conference on
Intelligent Robots and Systems
September 28 - October 2, 2004, Sendai, Japan

# High Sensitivity 2-D Force Sensor for Assembly of Surface MEMS Devices

Yantao Shen, Ning Xi, and U. C. Wejinya
Dept. of Electrical and Computer Engr.
Michigan State University
East Lansing, MI, USA
Email: {shenya,xin,wejinyau}@egr.msu.edu

Wen J. Li
Dept. of Automation and Computer-Aided Engr.
The Chinese University of Hong Kong
Shatin, Hong Kong, China
Email: wen@acae.cuhk.edu.hk

*Abstract*— **This paper aims at advancing micromanipulation technology with in situ polyvinylidene fluoride (PVDF) piezoelectric force sensing during microassembly and packaging process. Based on the previously developed PVDF 1-D sensor, by employing the parallel beam structure, a novel 2-D force sensor with relatively high natural frequency and sensitivity is optimally designed. The sensor can detect micro force and force rate signals which can be fed back so as to greatly improve the reliability of microassembly. Preliminary calibration and experimental results on assembly of surface MEMS devices both verified the performance of the new 2-D sensor that demonstrates a high sensitivity and a resolution in the range of $\mu$N. Ultimately the technology will provide a critical and major step towards the development of automated micro-manufacturing processes for batch assembly of micro devices.**

## I. Introduction

The processes of quickly and cheaply assembling MEMS devices have not been developed, partly because, at the micro-scale, structures are fragile and easily breakable. They typically break at the micro-Newton ($\mu$N) force range– a range that cannot be felt by a human operator assembling microstructure with tweezers and microscopes, and is also not reliably measurable by the existing force sensors during assembly. As a result, it is extremely difficult to manipulate parts for assembly at that scale. Moreover, this situation decreases overall yield and drives up cost of MEMS [1].

For these reasons, various force sensing mechanisms have already been investigated in sensing contact force during microassembly [2][3][4]. In a summary, for strain gauges and piezoresistive effect, piezomagnetic effect, and capacitive sensors, their resolutions are in the range of sub-mN or mN. Although optical techniques have high resolution in the range of nano Newton (nN), comparing to other methods, they are more expensive and have narrow dynamic range. Fortunately, it can be found that the piezoelectric polymer film PVDF (Polyvinylidene Fluoride) has a low modulus but with a relatively high electromechanical coupling coefficient, as a result, PVDF could be an ideal force transduction material for micro force sensing. These properties are important for developing a high sensitivity 2D micro force sensor in this paper.

The objective of this paper is to discuss possibly the most feasible and versatile solution in force sensing for microassembly, i.e., the use of PVDF-based cantilever structure as a sensing device during the process of microassembly which was briefly presented in [5][6]. Based on the piezoelectric effect and the parallel-beam structure, we developed both the theoretical model and the prototype structure of a novel 2-D PVDF high sensitivity force sensor. By integrating the PVDF-based force sensor on a probe-tip of micromanipulator for microassembly, the micro contact force and force rate signals can be extracted and amplified by a custom-built electronic circuit, which could be fed back for regulating the micro contact force/impact to a safe margin on-line during microassembly. To verify the effectiveness of model, the calibration of sensor had been implemented using a high resoution and precisely calibrated 100x optical microscope and CCD system. The microscope can measure the tiny bending angle or deflection of the sensor beam in real time when micro force is exerted. As a result, the actual exerted force can be achieved. Preliminary calibration results clearly indicate the effectiveness of the developed 2-D force sensor which has high sensitivity and a resolution in the range of $\mu$N. Furthermore, sensing experiments on assembly of surface MEMS devices (micro mirrors) prove that the sensor can be used for automated microassembly, resulting in higher and faster yield in assembling surface micromachining structures.

## II. Design and Modelling of 2-D Force Sensor

### A. Sensor Model

Fig.1 shows the physical model of a 1-piece PVDF film sensor. Based on piezoelectric effect [7], the mechanics of materials for cantilever beam [8], and an equivalent circuit model of a resistor $R_P$ in parallel with a capacitor $C_P$ for the PVDF film, the output voltage $V(t)$ across the PVDF film due to charge $Q(t)$ generated by external micro force $F(t)$, can be described by [6]

$$\frac{V(t)}{R_P} + \dot{V}(t)C_P = \frac{dQ}{dt}. \quad (1)$$

Thus we have the following equation to represent the relationship between the generated voltage and the contact force:

$$V(t) + \lambda \dot{V}(t) = B\dot{F}(t) \quad (2)$$

0-7803-8463-6/04/$20.00 ©2004 IEEE

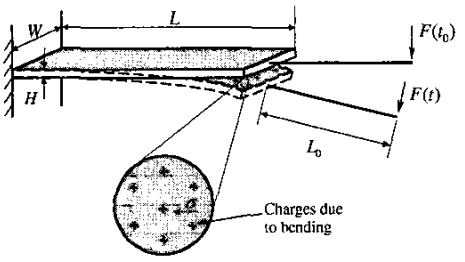


Fig. 1. Illustration of the force sensor using 1-piece PVDF film.

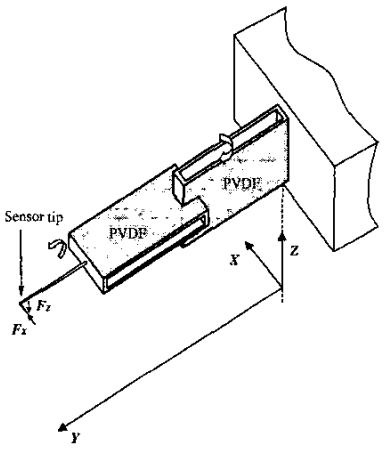


Fig. 2. Illustration of the 2-D force sensor.

where $\lambda = R_P C_P$ is a constant. $B = \dfrac{R_P A d_{31} H (L_0 + \frac{L}{2})}{2I}$ is constant. $A$ is surface area ($L \times W$). $d_{31}$ is transverse piezoelectric coefficient. $I$ denotes the inertial moment of cross-sectional area $a$ ($W \times H$) of PVDF film.

To follow the design and model of the 1-piece PVDF sensor, a self-decoupling 2-D PVDF force sensor is designed as shown in Figure 2.

It is designed based on a parallel beam structure as shown in Fig. 3. In each direction, two pieces of PVDF films are used to construct a 2-piece parallel beam so that the rigidity of the structure can be improved. Meanwhile, due to two PVDF films are used for each dimension, comparing to the 1-piece PVDF film, the sensitivity of the force sensing in that direction can be degraded a little. As shown in Fig. 2, two parallel beams are aligned perpendicularly to each other, so this structure provides a

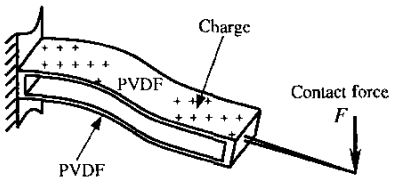


Fig. 3. Illustration of the parallel beam structure.

decoupled force measurement in the X and Z directions. Based on equation (2), the decoupled output voltages and forces of the 2-D sensor can be described as

$$\begin{aligned} V_Z(t) + \lambda_Z \dot{V}_Z(t) &= B_Z \dot{F}_Z(t) \\ V_X(t) + \lambda_X \dot{V}_X(t) &= B_X \dot{F}_X(t) \end{aligned} \tag{3}$$

where $\lambda_Z = \lambda_X = R_P C_P$.

$$B_Z = \frac{R_P}{2} \underbrace{\frac{2 A d_{31} (2H + d)(L_0 + \frac{L}{2})}{2 I_d}}_{\beta_Z}.$$

$$B_X = \frac{R_P}{2} \underbrace{\frac{2 A d_{31} (2H + d)(L_0 + \frac{3L}{2})}{2 I_d}}_{\beta_X}.$$

$I_d = 2I + \dfrac{a(d^2 + H^2)}{2}$ is the inertia moment of parallel beam. $d$ is the gap distance between the two parallel PVDF films.

### *B. Signal Conditioning and Transfer Function*

Preprocessing of sensed data is critical by the circuit for two reasons: (i) to remove any noise, and (ii) to amplify and extract the desired signal which is in this case the force. The schematics of developed circuit is shown in Figure 4.

In this circuit, a differential charge amplifier is designed for the PVDF force sensor. The differential charge amplifier is based on the chopper stabilized operational amplifier TC7650C with a high input impedance $10^{12}\Omega$ and low bias current $1.5pA$. A high input impedance can avoid bleed-off of the charge on the feedback capacitor $C_{f1}$ and $C_{f2}$, and low bias current prevents the feedback capacitor from charging and discharging at excessive rates. Following the charge amplifier, a differential-to-single-ended amplifier is added. In this design, the total differential topology can reduce the common mode noises more effectively. In other words, by choosing the charge amplifier, the cable capacitors $C_c$ are removed from the dynamic model of the circuit, then a long cable can be used to connect the sensor and the circuit without affecting the system sensitivity. To reject the existing high frequency noises, an active low pass filter with suitable cutoff frequency is used before the voltage output. The integration of the output voltage by time can also be achieved by an integrator unit in the circuit. In addition, the reductions of RFI (Radio Frequency Interference) and EMI (Electromagnetic Interference) are handled by the related filtering and shielding in the circuit. Small cable resistors $R_{c1}$ and $R_{c2}$ can provide ESD (Electrostatic discharge) protection. Besides signal processing in the hardware, to further remove the noises from the data acquisition system, a Gaussian-type low pass filter was added in the data collection program, that is,

$$\begin{cases} s_f(i) = \sum_{j=-k}^{k} r e^{-j/\alpha} s(i+j) \\ \sum_{j=-k}^{k} r e^{-j/\alpha} = 1 \end{cases} \tag{4}$$

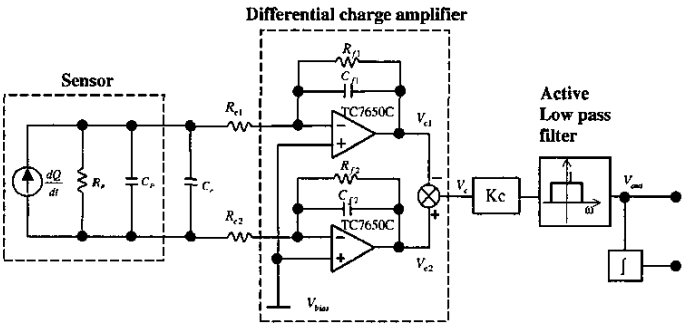


Fig. 4. Schematics of the electronic circuit.

where $\alpha$ is a small constant and $k$ is a positive integer (*i.e.* $k = 5$). $r$ is a gain. $s_f(i)$ is the filtered signal at the $ith$ sampling point, $s(\cdot)$ is the collected signal.

As shown in Fig. 4, the output voltage of the Z or X sensing direction from the differential charge amplifier is as follows,

$$\begin{aligned} V_c(s) &= V_{c2}(s) - V_{c1}(s) \\ &= 2I_Q(s)Z_f(s) \end{aligned} \tag{5}$$

where $R_{f1} = R_{f2} = R_f$. $C_{f1} = C_{f2} = C_f$. $I_Q(s) = \beta_{(\cdot)}F_{(\cdot)}(s)s$. $\beta_{(\cdot)}$ represents the $\beta_Z$ or $\beta_X$. $F_{(\cdot)}(s)$ denotes the $F_Z(s)$ or $F_X(s)$. $Z_f(s) = \dfrac{R_f}{1 + R_f C_f s}$.

By considering the whole circuit, the transfer function is then given by

$$\frac{V_{out}(s)}{V_c(s)} = \frac{K_c}{1 + \tau_1 s} \tag{6}$$

where $K_c$ is the gain of the differential-to-single-ended amplifier. $\tau_1$ is time constant of the active low pass filter.

Finally, from eqns. (5) and (6), the global transfer function of each dimension of the 2-D sensor is

$$GT(s) = \frac{V_{out}(s)}{F_{(\cdot)}(s)} \doteq \frac{2K_c\beta_{(\cdot)}}{C_f} \frac{\tau s}{(1 + \tau s)(1 + \tau_1 s)}. \tag{7}$$

The function of the equation is a bandpass type filter. $\tau = R_f C_f$ is the time constant. Since $\tau_1$ is very small in the circuit (*i.e.* 0.001), eqn.(7) can be rewritten as

$$GT(s) = \frac{V_{out}(s)}{F_{(\cdot)}(s)} \doteq \frac{2K_c\beta_{(\cdot)}}{C_f} \frac{\tau s}{(1 + \tau s)}. \tag{8}$$

From this equation, the force rate can be achieved. By inverse Laplace transformation of eqn. (8), and then integrating both sides of the new equation by time, we can obtain the micro contact force of each dimension by measuring the output voltage $V_{out}(t)$ of each dimension of the 2-D sensor, when the initial values $F_{(\cdot)}(t_0)$ and $V_{out}(t_0)$ are known.

$$F_{(\cdot)}(t) - F_{(\cdot)}(t_0) = \frac{1}{2K_c\beta_{(\cdot)}R_f}[\tau(V_{out}(t) - V_{out}(t_0)) + \int_{t_o}^{t} V_{out}(t)dt] \tag{9}$$

Using the principle of vector triangle, we can calculate a 2-D resultant force at the contact tip of sensor in real time after obtaining $F_Z(t)$ and $F_X(t)$, that is

$$\begin{cases} \|F(t)\| = \sqrt{F_Z(t)^2 + F_X(t)^2} \\ \theta_F = \tan^{-1}(\dfrac{F_Z}{F_X}). \end{cases} \tag{10}$$

### C. Optimal Design and Analysis of 2-D Sensor

Back to the sensor mechanical model, considering the bending shape of the sensor beam is only first mode shape, then the natural frequency of each dimension beam of the 2-D sensor will be as follows [8].

$$f_{n2} \approx \frac{1}{2\pi}\sqrt{\frac{3EI_d}{(0.2235\rho_s L + m_t)L^3}} \tag{11}$$

where $\rho_s$ is the mass density of the sensor beam along the length, $m_t$ is the mass of the sensor tip. Substituting the values into eqn. 11, the natural frequency of the 2-D sensor is about $193.8Hz$ when $d = 0$. While the natural frequency of the 1-piece cantilever beam is about $f_{n1} = \dfrac{1}{2\pi}\sqrt{\dfrac{3EI}{(0.2235\rho_s L + m_t)L^3}} = 68.7Hz$. Obviously, the natural frequency of the 2-D sensor is improved by using the parallel beam structure.

Besides the natural frequency, to compare to the sensitivity of the 1-piece PVDF force sensor as shown in Fig. 1, the sensitivity of the 2-D sensor is degraded in general. If the gap distance $d$ is reduced, the sensitivity of the 2-D sensor can be increased limitedly. For instance, when no gap exists, the sensitivity will be a maximum value for this 2-piece parallel beams structure, that is $\dfrac{8I}{2I + \dfrac{aH^2}{2}} \dfrac{K_c B}{R_P C_f}$, while the 1-piece is $\dfrac{2K_c B}{R_P C_f}$. The sensitivity of the 2-D sensor can be half of that of 1-piece PVDF sensor. Here, the sensitivity of the 2D force sensor doesn't degrade much more due to the use of double piece PVDF films at each sensing dimension. We can improve the sensitivity of the 2-D sensor system by adjusting the gain $K_c$.

If we choose 3-piece, 4-piece or multi-piece PVDF films other than 2-piece to build the parallel beam sensor, although the performance of anti-vibration is improved, the

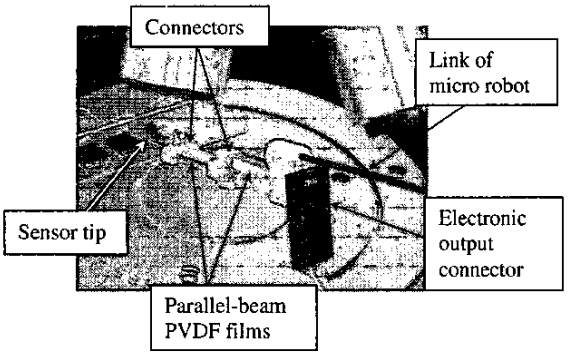


Fig. 5. Prototype of the 2-D sensor.

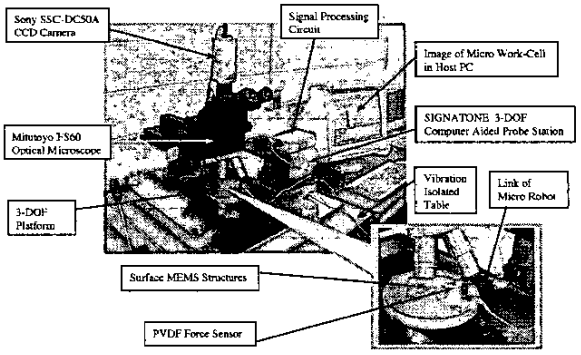


Fig. 6. A micro robotic system at MSU.

sensitivity of the sensor is degraded greatly. For example, if we stack all pieces together ($d = 0$), the sensitivity of this multi-piece sensor will be as follows.

$$K_s(j = 2i - 1) = \frac{2j^2 I}{jI + \sum_{n=1}^{\frac{j+1}{2}} 2a(n-1)^2 H^2} \frac{K_c B}{R_P C_f} \quad i = 2, 3, 4, \ldots \quad (12)$$

and

$$K_s(j = 2i) = \frac{2j^2 I}{jI + \sum_{n=1}^{\frac{j}{2}} 2a(n-\frac{1}{2})^2 H^2} \frac{K_c B}{R_P C_f} \quad i = 1, 2, 3, \ldots \quad (13)$$

where $j$ represents the piece number of the PVDF films. From eqns. (12) and (13), upon the consideration of the highest sensitivity of sensor as well as a higher natural frequency, we can determine the maximum sensitivity by the following approach:

$$\frac{\partial K_s(j)}{\partial j} = 0. \quad (14)$$

Then the 2-piece design is the optimal solution among the multi-piece parallel beam structures.

## III. Calibration and Experiment

### A. Sensor Prototypes

Referring to the basic physical model of the 2-D PVDF sensor, Fig. 5 shows the prototypes of the PVDF sensor used in the calibration and experiments. As shown in figure, the PVDF film has the following dimensions and parameters: $L_0 = 0.0225m; L = 0.0192m; W = 0.0102m$; $H = 28\mu$m; $R_P = 1.93 \times 10^{12}\Omega$; $C_P = 0.90 \times 10^{-9}F; E = 2 \times 10^9 N/m^2, d_{31} = 23 \times 10^{-12}C/N$. $R_f = 5 \times 10^9\Omega$. $C_f = 0.2 \times 10^{-10}F$.

In addition, the pyroelectric effect of the PVDF film is need to be considered. Since the PVDF film was coated by very thin Acrylic protective layers which are the thermal insulation, and therefore the pyroelectric effect within the sensor is reduced.

### B. Set-up

The experimental evaluation of the theoretical analysis were conducted in the Robotics and Automation Laboratory at Michigan State University. In the laboratory, a micro robotic system, as shown in Figure 6, was used for the calibration and experiment work. It consists of a 3-DOF micromanipulator (SIGNATONE Computer Aided Probe Station), a 3-DOF platform, a Mitutoyo FS60 optical microscope and a Sony SSC-DC50A CCD Color Video Camera. The micro robot is controlled by a PC-based control system. The robotic system is an open platform which can easily be equipped with the PVDF force sensing system. Several motion control software and user interface have been developed. They provide a flexible and user-friendly platform to integrate with the micro force sensing system and control software. When the micro force is detected by the PVDF sensor, the output voltage signals from the electronic circuit could be collected via a multifunction analog/digital input/output board (AX5411H) into a PC. There exists a force data communication between the PC and micro robotic system. The sampling frequency of the AX5411H is about 1KHz in the experiments. To reduce vibrations, an active vibration isolated table was used during the calibrations and experiments. Within the set-up, the proposed calibration method and experimental studies was conducted to test the performance of the developed 2-D force sensing system at a stable room temperature.

### C. Calibration

Based on the strain energy relation due to bending of cantilever beam [8], we have the relationship between the micro contact force and deformations such as tiny bending angle and deflection at the free end of the 2-D sensor beam as follows.

$$\theta(t) = \frac{\partial U}{\partial M_0} \approx sin(\theta) \quad (15)$$

where $U = \frac{1}{2EI_d} \int_0^L [-FL_0 - F(L-x)]^2 dx$ represents the strain energy due to bending. $I_d$ is the moment of inertia of the parallel beam of the sensor. $M_0 = F(t)L_0$ is the bending moment at the free end of the PVDF parallel beam.

Moreover, we get the deflection at the rigid tip

$$\delta(t) = \frac{\partial U}{\partial F} + \frac{\partial U}{\partial M_0} sin(\theta) \tag{16}$$

From the equations (15) and (16), then the actual force can be calculated by the following equation if $\theta(t)$ or $\delta(t)$ is accurately measured and $EI_d, L, L_0$ are perfectly known:

$$F(t) = \frac{2EI_d\theta(t)}{L^2 + 2LL_0} \tag{17}$$

or

$$F(t) = \frac{3EI_d\delta(t)}{L^3 + 3L^2L_0 + 3L_0^2L}. \tag{18}$$

Without loss of generality, assume $EI_d, L, L_0$ are the known constants. By virtue of a precisely calibrated Mitutoyo 100x microscope (with a 50x objective and a 2x zoom), and a Sony CCD camera system, the set-up for accurately measuring the tiny bending angle $\theta(t)$ or deflection $\delta(t)$ of the sensor beam under the microscope was built. The total resolution of the set-up approaches 0.2106$\mu$m/pixels in X and 0.2666$\mu$m/pixels in Y on the image plane. Notice that, to obtain an accurate $\theta(t)$ or $\delta(t)$ from the captured image, image processing techniques and least square method were adopted to find an optimal solution on $\theta(t)$ or $\delta(t)$. Meanwhile, based on the model in eqns. (9) and (10), the output voltage signals transferred by the designed circuit can be used to calculate the theoretical value of micro contact force. By preliminary calibration, the sensitivity of the 2-D sensor was 2.3985V/$\mu$N ($d$=0), the resolution of the sensor was in the range of $\mu$N.

As an important aspect of the sensor, dynamic range is an ability to respond to signals having both large and small amplitude variation. The output width of sensor system is 12 volts with a quantization resolution of 0.73 mV, therefore the output dynamic range of 2-D sensor is 84.3 dB. The input resolution of the sensor approaches $10^{-7}$ Newton. In analogy with output dynamic range, the input dynamic range is thus given by the ratio of input width to the input resolution. By calibration, when deflection of the sensor tip approaches 90°, the input dynamic range of the 2-D sensor was estimated to be 121.9 dB.

### *D. Force Sensing*

Experiments on the contact sensing is first conducted. By using the 2-D sensor, a contact-stop sensing experiment is implemented when the sensor tip acts on a planar glass surface that is set up an angle of 75 degree around Y with respect to the ZY plane (see the coordinate in Figure 2). The set-up means $F_Z = Fcos15°$ and $F_X = Fcos75°$. The 2-D force signals recorded are plotted in Fig.7 ($F_Z \approx 3.7F_X$ in the plot). The result verifies the performance of sensing and self-decoupling of the 2-D force sensor.

### *E. Force Sensing on Assembly of Surface MEMS Device*

Furthermore, the contact forces from the 2-D sensor were also tested when the contact tip of the sensor lifts up a micro mirror on the MUMPs43 chip. The micro mirror components usually lie on the surface of substrate after fabrication processes. Before being an effective optical switch, an assembly process is needed to lift it up to an upright position without breaking them. In this experiment, a 2-D PVDF sensor, was mounted at the front of a micro manipulator. Before lift-up, the sensor tip was first moved to the initial position under the micro mirror, then the tip position was controlled to move forward in 1.0mm/s and to move upward in 0.60mm/s simultaneously. As a result, the tip begins to lift the micro mirror up until the mirror approaches an upright position. The top views of the sequence of assembly of micro mirror are shown in Figure 8. The size of the micro mirror is about 300$\mu$m ×300$\mu$m.

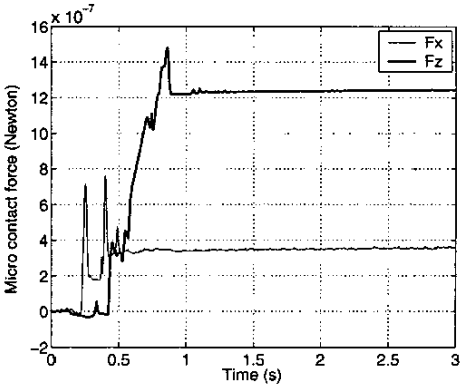


Fig. 7. 2-D sensor responses when force exerting along 75 degree with respect to the ZY plane.

During lift-up, gravity force is not a dominant force in micro environment, so the forces exerted on the tip are mainly from the counteraction moments of the hinges and the latches, the friction forces when the tip slides down on the bottom surface of the mirror and the small adhesion forces. Figure 9 gives an illustration of the assembly forces acting on a micro mirror during lift-up by the sensor tip. According to the force analysis in Figure 9, the friction force $F_f$ can be decomposed as the $F_{fx}$ and $F_{fz}$, the counteraction force $F_n$ has the components $F_{nx}$ and $F_{nz}$, so the micro contact forces $F_X$ and $F_Z$ can be approximately denoted as:

$$F_X = F_{nx} + F_{fx}$$
$$F_Z = F_{nz} - F_{fz}.$$

Referring to Figure 9, Fig.10(a) shows the filtering results of the $F_Z$ and $F_X$ sensed by the 2-D force sensor. In the Fig.10(a), before the tip stops, a downward in the force $F_Z$ plot indicates that the $F_Z$ decreases when the mirror is approaching the upright position, while $F_X$ is increasing due to the increasing counter force and moments from the hinges and latches (see Fig. 8(iv) and (v)). After stopping the motion control (correspond to Fig. 8(vi)), due to the friction force $F_f$ vanishes, the contact force $F_Z$ has a continual and slow increase as well as $F_X$ has a decrease until the tip motion stops finally (two forces approach the constants). Figure 10(b) is the tip positions in Z and X during lift-up. The experimental results meet

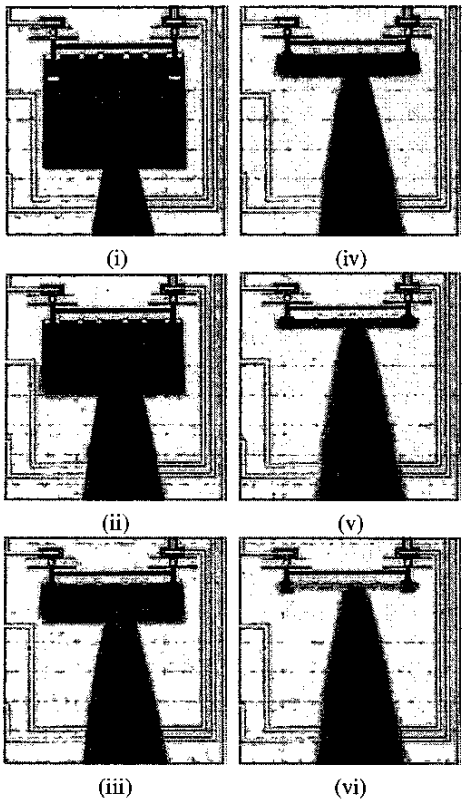


Fig. 8. Top views of the 2-D sensor tip lifting up a micro mirror.

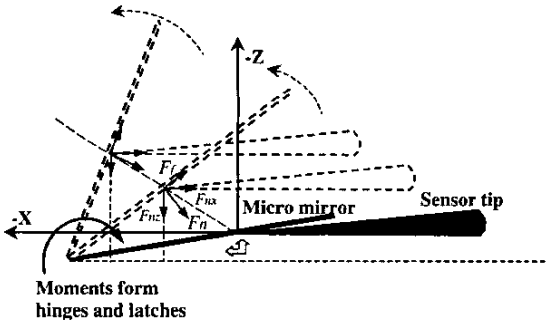


Fig. 9. Illustration forces acting on a micro mirror during lift-up process.

the theoretical analysis of contact force during lift-up. The results also confirm the performance of the developed 2-D high sensitivity force sensor.

## IV. Conclusions

In this paper, we used polyvinylidene fluoride (PVDF) to fabricate high sensitivity force sensory system for assembly of surface MEMS devices. Based on the electronic and mechanical models of PVDF film, by adopting the parallel beam structure, a novel high sensitivity 2-D force sensor is designed and optimally analyzed. Preliminary calibration and experimental results verified the performance of the

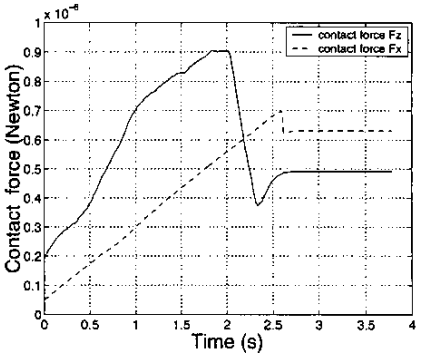


(a) Micro contact forces: $F_Z$ and $F_X$

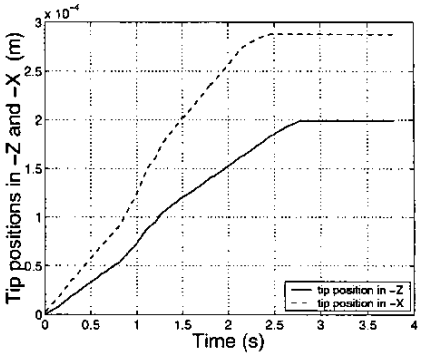


(b) Tip positions in -Z and -X

Fig. 10. 2D force sensing experiment on lifting up a micro mirror.

new 2-D sensor that shows a high sensitivity and a resolution in the range of $\mu$N. After refining the model in future work, ultimately the technology will provide a critical and major step towards the development of automated micro-manufacturing processes for batch assembly of MEMS devices.

## References

[1] S. K. Koelemijer, L. Benmayor, J. -M. Uehlinger and J. Jacot, *Cost Effective Micro-System Assembly Automation*. Proceedings of 1999 Emerging Technologies and Factory Automation, Vol. 1. pp. 359-366, 1999.

[2] S. Fatikow, J. Seyfried, ST. Fahlbusch, A. Buerkle and F. Schmoeckel, *A Flexible Microrobot-Based Microassembly Station*, Journal of Intelligent and Robotic Systems, Vol. 27, pp. 135-169, 2000.

[3] B. Nelson, Y. Zhou and B. Vikramaditya, *Sensor-Based Micro-Assembly of Hybrid MEMS Devices*, IEEE Control System Magazine, Vol. 18, no.6 pp. 35-45, 1998.

[4] M. Greminger, Y. Ge and B. Nelson. *Sensing nanonewton level forces by visually tracking structural deformations*. ICRA 2002, pp.1943-1948, 2002.

[5] C. K. M. Fung, I. Elhajj, W. J. Li, and N. Xi, *A 2-D PVDF Force Sensing System for Micro-manipulation and Micro-assembly*, Proc. of the IEEE International Conference on Robotics and Automation, pp. 1489-1494, 2002

[6] Y. T. Shen, N. Xi, and Wen J. Li, *Force Guided Assembly of Micro Mirrors*, Proceedings of the IEEE/RSJ International Conference on Intelligent Robots and Systems, Vol. 3, pp. 2149-2154, 2003.

[7] *An American National Standard: IEEE Standard on Piezoelectricity*, ANS/IEEE Std 176-1987, 1987.

[8] W. H. Bowes, L. T. Russell, and G. T. Suter, *Mechanics of Engineering Materials*. John Wiley & Son. 1984.